International Journal of Heat and Mass Transfer 52 (2009) 2009–2017

Contents lists available at ScienceDirect

International Journal of Heat and Mass Transfer

journal homepage: www.elsevier.com/locate/ijhmt

Thermal performance of dimpled surfaces in laminar flows

Nian Xiao [a], Qiang Zhang [b], Phillip M. Ligrani [b,*], Rajiv Mongia [c]

[a] Department of Mechanical Engineering, University of Utah, Salt Lake City, UT 84112-9208, USA
[b] Department of Engineering Science, University of Oxford, Oxford OX1 3PJ, UK
[c] Intel Corporation, 2200 Mission College Blvd, Santa Clara, CA 95054-1549, USA

ARTICLE INFO

Article history:
Received 2 October 2007
Available online 26 December 2008

ABSTRACT

The present study provides data which illustrate the effects of an array of dimples on local and spatially-averaged surface Nusselt number distributions, as well as on friction factors in channels with *laminar flow*. Trends of spatially-averaged Nusselt numbers and friction factors are provided as they vary with dimple depth, channel height, Reynolds number from 260 to 1030, and the use of protrusions on the opposite channel wall. When compared with turbulent flow results, the present laminar data illustrate changes due to the absence of turbulence transport. For example, in contrast to turbulent flows, the present laminar flow data show that there is no overall benefit from the use of a top wall with protrusions. In addition, spatially-averaged Nusselt number ratios and friction factor ratios measured on a deep dimpled surface with a smooth top wall show trends which are opposite from ones observed in turbulent flows, since lower laminar heat transfer augmentations are present for smaller channel heights when compared at the same Reynolds number.

1. Introduction

Surface dimples produce substantial surface heat transfer augmentations with relatively small pressure drop penalties in internal passages. As such, arrays of surface dimples are useful for a variety of practical applications, such as electronics cooling, heat exchangers, turbine blade internal cooling passages, micro-scale passages, bio-medical devices, and combustion chamber liners. Of several early studies (mostly conducted in Russia), Murzin et al. [1] describe the flow over and within shallow spherical depressions and conclude that this flow is mostly symmetric, with stable re-circulatory flows inside of the depressions. Kesarev and Kozlov [2] present distributions of local heat transfer coefficients inside of a single hemispherical cavity and indicate that the convective heat transfer from the cavity is higher, especially on the downstream portion, than that from the surface of a plane circle of the same diameter as the cavity diameter. Afanasyev et al. [3] experimentally studied the heat transfer enhancement mechanism for flows in a dimpled channel with several different shapes. Enhancements of 30–40%, with pressure losses that are not increased appreciably relative to a smooth surface, are reported. Terekhov et al. [4] present experimental measurements of flow structure, pressure fields, and heat transfer in a channel with a single dimple on one surface. According to the authors, pressure losses increase (compared to a smooth wall) with an increase of cavity depth and decrease as the Reynolds number increases. Cavity heat transfer enhancements are also noted, especially for shallow holes, mainly as a result of an increase in heat transfer area and the changes to flow structure produced by the dimple.

More recent investigations conducted in the USA include the one described by Chyu et al. [5], who present local heat transfer coefficient distributions on surfaces imprinted with staggered arrays of two different shapes of concavities. Over a range of Reynolds numbers, enhancement of the overall heat transfer rate is about 2.5 times smooth surface values, and friction factors are about half the values produced by conventional rib turbulators. Moon et al. [6] give data that show that improvements in heat transfer intensification and pressure losses remain at approximately constant levels for different Reynolds numbers and channel heights.

Ligrani et al. [7] discuss flow structure and local Nusselt number variations in a channel with dimples and protrusions on opposite channel walls. Instantaneous flow visualization images and surveys of time-averaged flow structure show that the protrusions result in added vortical, secondary flow structures and flow mixing. As a result, local friction factors and Nusselt numbers are augmented compared to a channel with no protrusions on the top wall. Mahmood et al. [8] indicate that important Nusselt number variations are observed as the array of protrusions is changed with respect to the locations of the dimples. With protrusions, form drag and channel friction are increased. As a result, thermal performance parameters are then generally slightly lower when protrusions and dimples are employed, compared to a channel with a smooth-dimple arrangement. Ligrani et al. [9] report detailed flow structural characteristics, including

* Corresponding author.
E-mail address: p_ligrani@msn.com (P.M. Ligrani).

0017-9310/$ - see front matter © 2008 Elsevier Ltd. All rights reserved.
doi:10.1016/j.ijheatmasstransfer.2008.11.006

Nomenclature

A_d	dimple surface area
A_0	projected smooth surface area
D	dimple print diameter
D_h	channel hydraulic diameter
F	spatially-averaged channel friction factor
f_0	baseline friction factor measured in a channel with smooth surfaces and no dimples
FOM	figure of merit, $(Nu/Nu_0)/(f/f_0)^2$
H	channel height
h'	local heat transfer coefficient based on flat projected surface area, $\dot{Q}''_0/(T_w - T_{mx})$
h	spatially-averaged heat transfer coefficient based on flat projected surface area, $\dot{Q}''_0/(T_w - T_{mx})$
k	thermal conductivity
Nu'	local Nusselt number, $h'Dh/k$
Nu	spatially-averaged Nusselt number, hDh/k
Nu_0	baseline Nusselt number in a channel with smooth surfaces and no dimples
P	streamwise spacing of adjacent dimple rows
$\dot{Q}''_0$	surface heat flux
Re_H	Reynolds number based on channel height, $H\overline{U}/v$
S	streamwise spacing of every other dimple row
T_w	wall temperature
T_{mx}	local mixed-mean temperature
TPP	thermal performance parameter, $(Nu/Nu_0)/(f/f_0)$
$\bar{v}$	channel spatially-averaged velocity
X	streamwise coordinate measured from test section inlet
Y	normal coordinate measured from test surface dimple horizon
Z	spanwise coordinate measured from test section centerline

Greek symbols

v	kinematic viscosity
δ	dimple depth

behavior of the primary and secondary vortex pairs shed from the dimples on a channel surface. Flow structure characteristics above dimpled surface with different dimple depths in a channel are described by Won et al. [10].

Most existing archival papers which utilize dimpled surfaces consider turbulent flows at higher Reynolds numbers. Existing thermal performance data for dimpled surfaces in laminar flows are rare, even though such data are useful for applications such as electronic cooling, where lower Reynolds numbers and lower speeds are present. The present study is aimed at partially remedying this deficiency by providing a systematic set of data which illustrate the effects of dimples on local and spatially-averaged surface Nusselt number distributions, as well as on friction factors in channels with *laminar flow*. Of particular interest are the changes which occur because of the absence of turbulence transport. In some cases, vastly different trends are present as flow conditions are altered, or as some aspect of channel geometry is changed. Two different dimple depths and three channel heights are employed at Reynolds numbers based on channel height ranging from 260 to 1030. Also included are laminar flow experimental results, which illustrate the combined effects of dimples and protrusions as they are located on opposite channel walls.

2. Experimental apparatus and procedures

2.1. Flow channel and test surface

A schematic of the facility used for the present study is shown in Fig. 1. The air passes into a rectangular bell mouth inlet, followed by a honeycomb, two screens, and a two-dimensional nozzle with a contraction ratio of 10. This nozzles leads to a boundary layer bleed-off plenum, followed by an inlet duct, the test section, and the downstream duct. The channel heights of all three ducts are adjustable by moving the duct top plates. The test section is 411 mm in width and 1219 mm in length. A series of two plenums (0.9 m square and 0.75 m square) are installed between the downstream duct and a 102 mm inner diameter pipe, which is then connected to the intake of an ILG Industries 10P type centrifugal blower. An ASME standard orifice plate and a Setra Model 267 differential pressure transducer are employed to measure the air mass flow rate through the pipe (and the test section as well).

Fig. 2a presents geometric details of the dimpled test surface employed in the test section. In the present study, a total of 29 rows of dimples are employed in the streamwise direction, with 4 or 5 dimples in each row. The dimples are positioned on the surface in a staggered array. The dimpled test surfaces are manufactured by vacuum forming acrylic sheets over molds with shapes designed to produce arrays of protrusions or dimples with the appropriate spacings, depth, and height, as required. Also identified in Fig. 2a is the test section coordinate system employed for the study. Note that the y-coordinate is normal from the test surface. Fig. 2b shows the individual dimple geometry details for deep and shallow dimples investigated in the present study. For one complete period of dimpled-surface geometry, the area ratios between dimpled and smooth surface for the deep and shallow dimples are 1.216 and 1.024, respectively. Ligrani et al. [7] and Mahmood et al. [8] present additional details on the dimpled test surfaces employed in the present study.

In addition to a smooth test section (for baseline data), four different channel configurations are employed in the present study, as shown in Fig. 3. The first configuration has a dimpled bottom surface and a smooth top surface, and the second configuration has protrusions on the top wall and dimples on the bottom surface, with the dimples and protrusions aligned with each other. The top-dimpled protrusion pattern is shifted ½ dimple print diameter and one print diameter for the other two configurations. The local reductions in flow cross-section area for these different configurations are evident in Fig. 3a–d.

All exterior surfaces of the facility (between the heat exchanger and test section) are insulated with 2–3 layers of 2.54 cm thick,

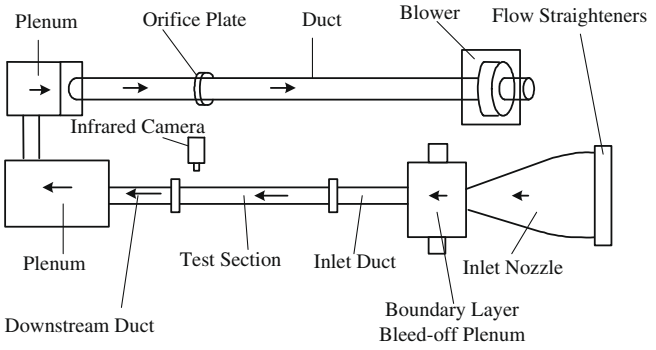

Fig. 1. Schematic diagram of the experimental apparatus.